JOURNAL OF COMPUTATIONAL PHYSICS 50, 138–161 (1983)

Tracing Complex Singularities with Spectral Methods

CATHERINE SULEM*

C.N.R.S., Département de Mathématiques, Université de Nice, France

AND

PIERRE-LOUIS SULEM† AND HÉLÈNE FRISCH

C.N.R.S., Observatoire de Nice, France

Received June 10, 1982

A numerical method for investigating the possibility of blow-up after a finite time is introduced for a large class of nonlinear evolution problems. With initial data analytic in the space variable(s), the solutions have for any $t > 0$ complex-space singularities at the edge of an analyticity strip of width $\delta(t)$. Loss of regularity corresponds to the vanishing of $\delta(t)$. Numerical integration by high resolution spectral methods reveals the large wavenumber behavior of the Fourier transform of the solutions, from which $\delta(t)$ is readily obtained. Its time evolution can be traced down to about one mesh length. By extrapolation of $\delta(t)$, such numerical experiments provide evidence suggesting finite-time blow-up or all-time regularity. The method is tested on the inviscid and viscous Burgers equations and is applied to the one-dimensional nonlinear Schrödinger equation with quartic potential and to the two-dimensional incompressible Euler equation, all with periodic boundary conditions. In the latter case evidence is found suggesting that existing all-time regularity results can be substantially sharpened.

I. INTRODUCTION

Proving all-time regularity or occurence of a singularity for nonlinear partial differential equations is often a mathematical challenge. This is especially true for problems with several space variables: it is still unknown for example whether the solution of the three-dimensional Euler equation for an incompressible fluid remains smooth for all times when it is so initialy. Even in one dimension, there are still a few open problems, e.g., the nonlinear Schrödinger equation with a sufficiently high nonlinearity in a periodic domain.

In various fields of nonlinear dynamics such as transition to chaos or dynamics of coherent structures, the computer, used in a heuristic mode, has greatly augmented our understanding of the mathematics [32]. Regularity problems are also amenable to numerical experimentation. Two different kinds of methods have been used up to now: Taylor series expansions in time and direct numerical simulations.

* Present address: Ben-Gurion University of the Neguev, Ber-Sheva, Israel.
† Present address: Tel-Aviv University, Ramat-Aviv, Israel.

0021-9991/83 $3.00

Methods of the first type have been introduced in critical phenomena [15] and are now employed in fluid dynamics [6, 23–25]. The solution of the problem is Taylor expanded in time around $t = 0$. The coefficients of the expansion are obtained recursively from the initial conditions. When the initial conditions are described by a finite number of rational Fourier modes, the accuracy of the coefficients is limited by round-off errors only. Several tens of coefficients may be computed in this way. Taylor series for various spatial integral norms of the derivatives (Sobolev norms or p-enstrophies), depending only on time, are generated from the Taylor series of the solution. The singularities of these norms are searched numerically at both real and complex times. The method is very reliable when the radius of convergence of the series is limited by a real-time singularity [23]. When it is limited by complex singularities, analytic continuation is required. The numerical implementation, which generally uses Padé approximants, may then be rather tricky [6, 24].

In methods of the second type, mainly used in fluid mechanics, the problem is solved numerically by time-marching techniques. Spectral methods are especially well adapted to problems with periodic boundary conditions. In addition to their high accuracy and the simplicity of their implementation, these methods preserve the continuity of the solution and of its derivatives of any order. Furthermore, the precision depends only on the resolution. Various quantities can yield informations on the regularity of the solution. One can, for example, consider Sobolev norms [27], but small truncation errors on the energy spectrum may lead to significant errors on norms of high index. One may also examine directly the analyticity properties of the solution. This is the approach used in this paper for solutions initially analytic in the space variables.

The idea of the method is to derive the width of the analyticity strip, i.e., the distance to the real domain of the nearest singularity, from the asymptotic behavior of the Fourier transform. This distance is only weakly dependent on the truncation wavenumber $k_{\max}$ if the Fourier modes retained for the analysis are sufficiently large to describe the asymptotic regime, but far enough away from $k_{\max}$. An extrapolation in time of the motion of these singularities yields predictions on regularity properties of the solution. Different situations may arise.

If a singularity reaches the real domain after a finite time t_*, the solution looses analyticity and becomes singular. A well-known example is the inviscid Burgers equation (Section IIIA). Numerical evidence for a similar behavior is obtained in this paper for the nonlinear Schrödinger equation with quartic potential (Section IV).

If the width of the analyticity strip is bounded away from zero, the solution is uniformly analytic (e.g., the viscous Burgers equation; Section IIIB). In this case, the minimum of the analyticity strip can be viewed as the smallest excited scale of the system.

A third possibility is that the system develops smaller and smaller scales, the solution remaining smooth for all times. This occurs when the width of the analyticity strip goes to zero without vanishing (e.g., exponential decay). Numerical simulations indicate that the Euler equation (Section V) and the MHD equation [13] in two dimensions display this kind of behavior. A one-dimensional example is given in [6].

It can be viewed as the advection of a passive scalar by a time-independent velocity field with a sinusoidal spatial dependency.

A general discussion of the relation between complex singularities and small scales properties of a flow can be found in [12, 14].

II. Implementation of the Numerical Method

We first recall the relation between the analytic properties of a function of one variable, defined in $\mathbb{R}$ or in a periodic domain, and the large wavenumber behavior of its Fourier transform.

Consider an analytic function $v(z)$ with singularities at complex location z_j, in the neighborhood of which it behaves as

$$v(z) \sim (z - z_j)^{\mu_j} \tag{2.1}$$

(μ_j is assumed not to be a positive integer). The behavior of the Fourier transform for $k \to +\infty$ is governed by the singularity of the upper half-space closest to the real domain that is not a multiple pole; if this singularity is located at $z_* = x_* + i\delta$ and has an exponent μ, one has

$$\hat{v}_k \sim |k|^{-(\mu+1)} e^{-k\delta} e^{ix_* k}, \qquad k \to +\infty. \tag{2.2}$$

A derivation of this property can be found in [7, p. 255]. It requires that $v(z)$ be growing not faster than an exponential as $|z| \to \infty$ and that the singularities be isolated points. Note that when several singularities are relevant asymptotically, $|\hat{v}_k|$ may display an oscillatory behavior.

Equation (2.2) shows in particular that for a function of one variable, the width of the analyticity strip is equal to the logarithmic decrement of the Fourier transform at large wavenumbers:

$$\ln |\hat{v}_k| \sim \delta k, \qquad k \to +\infty. \tag{2.3}$$

This property is not easily extended to functions of several variables. It is, however, easy to derive the following estimate [1]:

If a 2π-periodic function $v(z)$ is analytic in the strip $\mathcal{S}_\rho = \{|\operatorname{Im} \mathbf{z}| < \rho\}$ and continuous in the closure of $\mathcal{S}_\rho$, the Fourier coefficients satisfy

$$|\hat{v}_\mathbf{k}| \leqslant M e^{-|k|\rho}, \tag{2.4}$$

where $M = \sup_{\mathcal{S}_\rho} |v|$. Reciprocally, if (2.4) holds, the function v is analytic in the strip $\mathcal{S}_\rho$.

Slightly weaker results hold for the angle average "energy spectrum,"

$$E(K) = \sum_{K < k < K+1} |\hat{v}(\mathbf{k})|^2, \tag{2.5}$$

because the angular summation can introduce algebraic prefactors. If v is analytic in $\mathscr{S}_\rho$, then

$$E(K) \leqslant Ce^{-2(\rho-\varepsilon)K}, \tag{2.6}$$

where ε is an arbitrarily small positive number. Reciprocally, if

$$E(K) \leqslant Ce^{-2\rho K}, \tag{2.7}$$

then analyticity is insured in $\mathscr{S}_{\rho-\varepsilon}$.

Let us now turn to the implementation of the above properties in the context of numerical simulations by spectral (or pseudospectral) methods. These methods preserve the large wavenumber behavior of the Fourier transform provided the resolution is large enough. For a function of one variable which is analytic in a strip of width δ, the amplitude of the Fourier modes decreases faster than $e^{-\delta k}$. Hence, when the series is truncated at a maximum wavenumber $k_{\max}$, the truncation error is bounded by

$$\sum_{|k|>k_{\max}} ce^{-\delta k} = c\frac{e^{\delta k_{\max}}}{1-e^{-\delta}}. \tag{2.8}$$

The function will thus be accurately represented by the truncated Fourier series provided $k_{\max}$ is larger than $1/\delta$, or in other words, provided the logarithmic decrement is large compared to the mesh size.

As the numerical integration is carried on in time, either the logarithmic decrement is bounded away from zero by $\delta_{\min} > 0$ or it goes on decreasing. In the former case, the integration can be carried on for arbitrarily long times, provided the mesh size is substantially smaller than $\delta_{\min}$. In the latter case, the calculation should be stopped when the logarithmic decrement becomes of the order of the mesh size, because the uncertainty on the position of the closest singularity is then of the same order than its distance to the real domain. Then, from the available numerical data, one tries to extract a law describing the time dependence of the logarithmic decrement. If the spatial resolution is large enough, this law may be representative of the asymptotic behavior of $\delta(t)$ and can be extrapolated to $t \to \infty$ or $t \to t_*$, depending on the situation.

III. Two Test Problems: The Inviscid and Viscous Burgers Equations

A. *The inviscid problem*

The equation reads

$$\frac{\partial u}{\partial t} + u\frac{\partial u}{\partial x} = 0, \qquad u(x,0) = u_0(x), \qquad x \in [0, 2\pi]. \tag{3.1}$$

We assume the analytic initial condition

$$u_0(x) = -\sin x. \tag{3.2}$$

With this choice of initial condition, the solution develops a shock which appears at time $t = 1$ in $x = 0$. The Burgers equation implies that there is conservation of the velocity along the trajectories. Therefore in Lagrangian coordinates, the solution has the simple representation

$$u(x(a, t), t) = u_0(a) \tag{3.3}$$

with

$$x(a, t) = a + tu_0(a). \tag{3.4}$$

Here, a denotes the initial position of a fluid particle located in x at time t. This solution is easily continued to the complex domain by considering complex values A of the initial position. At time t, the position of a fluid particle located initially in A is

$$z(A, t) = A + tu_0(A). \tag{3.5}$$

The singularities of $u(z, t)$ are located at the points where trajectories intersect each other. They are thus given by the zeros of $\partial z/\partial A$. For initial condition (3.2), there are two complex conjugate singularities $z_* = \pm i\delta$ with

$$\delta(t) = \cosh^{-1}(1/t) - t \operatorname{sh}[\cosh^{-1}(1/t)]. \tag{3.6}$$

These singularities reach the real axis in $x_* = 0$ at time $t_* = 1$. The nature of the singularities is obtained by Taylor expanding the velocity around the singularity points [11]. As long as $\delta(t) \neq 0$,

$$u(z, t) \sim (z - z_*(t))^{1/2}. \tag{3.7}$$

When $\delta(t)$ vanishes, which occurs at $t = t_*$,

$$u(x_*, t) \sim (x - x_*)^{1/3}. \tag{3.8}$$

As a consequence, the large wavenumber behavior of the Fourier transform of the solution is given by

$$\hat{u}_k \sim k^{-3/2} e^{-\delta(t)k}, \qquad t < t_*, \tag{3.9}$$

$$\hat{u}_k \sim k^{-4/3}, \qquad t = t_*. \tag{3.10}$$

Remark. The $k^{-4/3}$ power law appears already before t_*. For $t < t_*$ the Fourier transform of the solution is given by (3.9) for $k \gg 1/\delta(t)$. For $1 \ll k \ll 1/\delta(t)$, it is of the form (3.10) [11], because this range of wavenumbers corresponds to a resolution for which the two complex conjugate singularities cannot be separated.

We now show that these properties can be obtained numerically. Equation (3.1) with initial condition (3.2) has been integrated using a dealiased pseudospectral method with a maximum wavenumber $k_{max} = 128$. Time stepping was done by a leap-frog scheme with mixing of even and odd time steps every 20 time steps [17]. The time step is 10^{-3}. The Fourier transform of the solution is plotted at various t in Fig. 1a (linear-log scales) and Fig. 1b (log–log scales). At early times, the exponential behavior occupies the major part of the wavenumber range. At later times, a power law behavior appears at small k and finally covers the whole wavenumber range at the singularity time. The upturn observed close to k_{max} comes from truncation errors.

More quantitative information is obtained by assuming for the Fourier transform of the solution an expression containing an exponential with a power law prefactor:

$$\hat{u}_k(t) = C(t)\, k^{-\alpha(t)} e^{-\delta(t)k}. \tag{3.11}$$

The adjustable parameters C, α, δ have been calculated with a least-squares method. Table I shows the values of α and δ for various values of time. Only the modes that have an amplitude larger than the level of the round-off error ($\sim 10^{-13}$) have been retained for the fit. There is a very good agreement between the exact and computed values of the logarithmic decrement as long as δ is larger than the mesh size. A two or three digit accuracy is achieved. For times $t < 0.6$, a fit in the range $5 \leqslant k \leqslant 100$ gives an exponent α close to 1.5 for the prefactor. During this period of time, the truncation errors are negligible. For longer times, the exponent decreases continuously to 1.37. This is due to the extension of the $k^{-4/3}$ power law to large wavenumbers (cf. the remark above). To obtain numerically the exponent of this power law at times close to the singularity ($0.9 \leqslant t \leqslant 1$), it is necessary to eliminate the exponential tail from the range of wavenumbers used for the fit. At $t \approx t_* = 1$, this tail has disappeared but the highest wavenumbers must now be excluded because of truncation errors. With a range limited to $2 \leqslant k \leqslant 30$, we have obtained values closed to $\frac{4}{3}$ (see Table I, fifth column).

B. *The viscous problem*

The viscous version of (3.1) with the same initial condition reads

$$\frac{\partial u}{\partial t} + u\frac{\partial u}{\partial x} = \nu \frac{\partial^2 u}{\partial x^2}, \qquad u_0(x) = -\sin x, \qquad x \in [0, 2\pi]. \tag{3.12}$$

For small ν, the solution develops a shock with a hyperbolic structure of the form

$$u(x) \sim -\tfrac{1}{2}\tanh(xH/4\nu). \tag{3.13}$$

The shock strength H is proportional to t^{-1}. Analytic continuation of the tanh shows that $u(z)$ has simple pole singularities at

$$z_n = \pm i(4\nu/H)(n + \tfrac{1}{2})\,\pi. \tag{3.14}$$

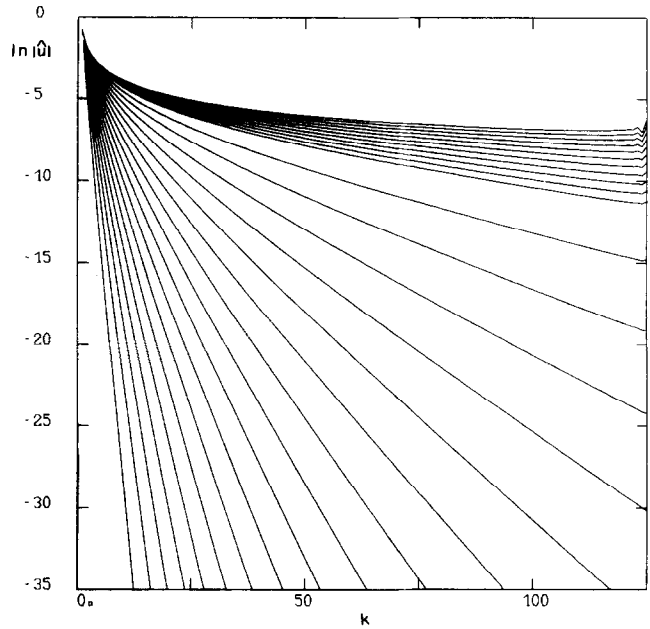

FIG. 1a. Fourier transform of the solution of the inviscid Burgers equation in linear–log scales at equally spaced times between $t = 0.05$ and $t = 0.9$ in steps of 0.05, and between $t = 0.91$ and $t = 1$ in steps of 0.01.

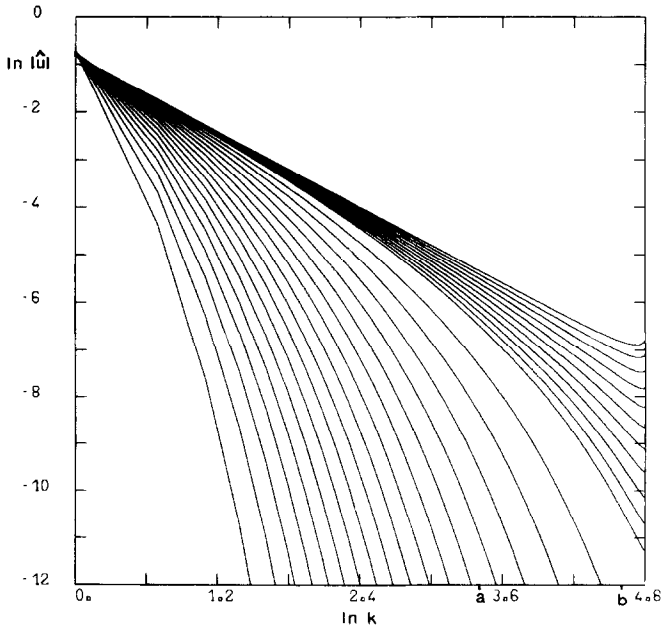

FIG. 1b. Same as Fig. 1a in log–log scales; $a = \ln 30$; $b = \ln 100$.

TABLE I

Inviscid Burgers Equation

t	Logarithmic decrement given by (3.6)	Fit of the numerical data with (3.11)		
		$5 \leqslant k \leqslant 100$		$2 \leqslant k \leqslant 30$
		δ	α	α
0.15	1.596	1.591	1.48	—
0.30	0.920	0.918	1.48	—
0.45	0.544	0.542	1.48	—
0.60	0.299	0.298	1.48	—
0.75	0.134	0.134	1.47	—
0.90	0.313 E–1	0.316 E–1	1.43	1.38
0.92	0.221 E–1	0.225 E–1	1.42	1.37
0.94	0.142 E–1	0.147 E–1	1.41	1.36
0.96	0.768 E–2	0.799 E–2	1.39	1.35
0.98	0.269 E–2	0.252 E–2	1.38	1.34
1.0	0	0.173 E–3	1.37	1.33

The asymptotic ($k \to \infty$) behavior of the spatial Fourier transform of the velocity is derived in [14] from the positions of the complex singularities. Two regimes can be distinguished,

an inertial range:

$$1 \ll k \ll H/\nu, \qquad \text{where} \quad \hat{u}_k \sim k^{-1}, \tag{3.15a}$$

a dissipation range:

$$k \gg H/\nu, \qquad \text{where} \quad \hat{u}_k \sim e^{(-2\pi\nu k/H)}. \tag{3.15b}$$

In the dissipation range, only the singularities closest to the real domain are relevant to leading order. In the inertial range, all the poles give a contribution and the k^{-1} behavior is obtained by summing a geometric series.

To solve (3.12) numerically, we have used a leapfrog scheme for the nonlinear term and a Crank–Nicolson scheme for the viscous term. We used $\nu = 5 \times 10^{-2}$. The Fourier transform of the solution is plotted in Fig. 2a (log–log scales) and in Fig. 2b (linear–log scales) at various times $t > 2$. Figure 2a shows a power law behavior at small wavenumbers and an exponential decay at large wavenumbers. This exponential is clearly seen in Fig. 2b. Table II gives the results of a fit of the Fourier transform with a function $C(t)\, k^{-\alpha(t)} e^{-\delta(t)k}$ in two ranges of wavenumbers, $2 \leqslant k \leqslant 10$ and $15 \leqslant k \leqslant 120$. In the first range, we can see the k^{-1} regime up to $t \approx 2$. Later, the behavior becomes exponential. In the second range of wavenumbers, α is very small, indicating that the complex singularities are simple poles. The logarithmic decrement

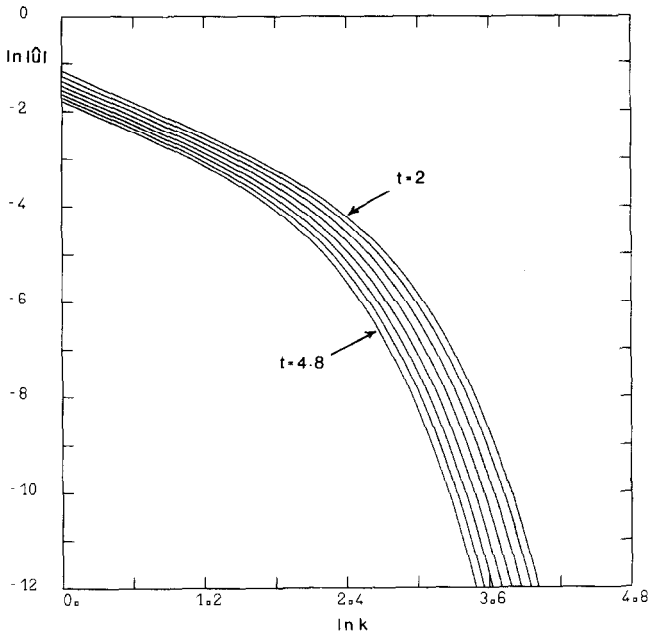

FIG. 2a. Fourier transform of the solution of the viscous Burgers equation ($\nu = 0.05$) in log–log scales at equally spaced times between $t = 2$ and $t = 4.8$ in steps of 0.4.

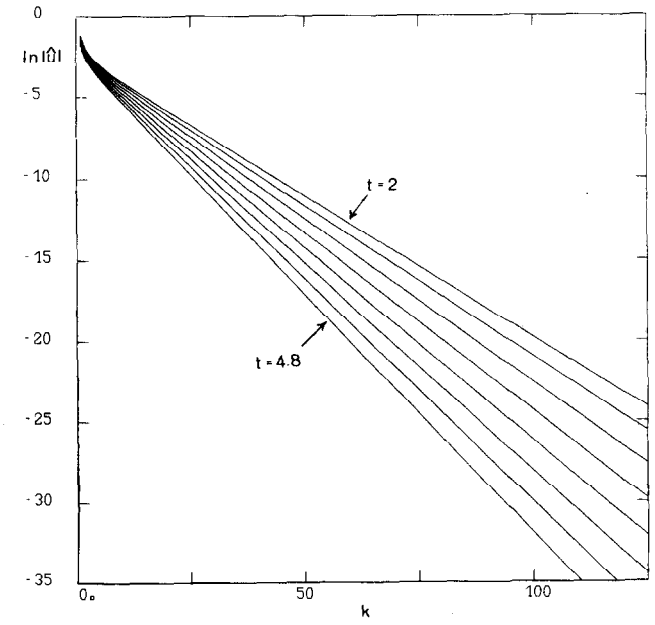

FIG. 2b. Same as Fig. 2a in linear-log scales.

TABLE II

Viscous Burgers Equation

	α	
t	$2 \leqslant k \leqslant 10$	$15 \leqslant k \leqslant 120$
0.8	1.2	2.3 E–2
1.2	1.1	1.0 E–2
1.6	1.0	6.8 E–3
2.0	0.96	4.4 E–3
2.4	0.91	2.1 E–3
2.8	—	−1.3 E–4
3.2	—	−2.8 E–4
3.6	—	−3.5 E–3
4.0	—	−1.4 E–3
4.4	—	1.8 E–3
4.8	—	2.3 E–4

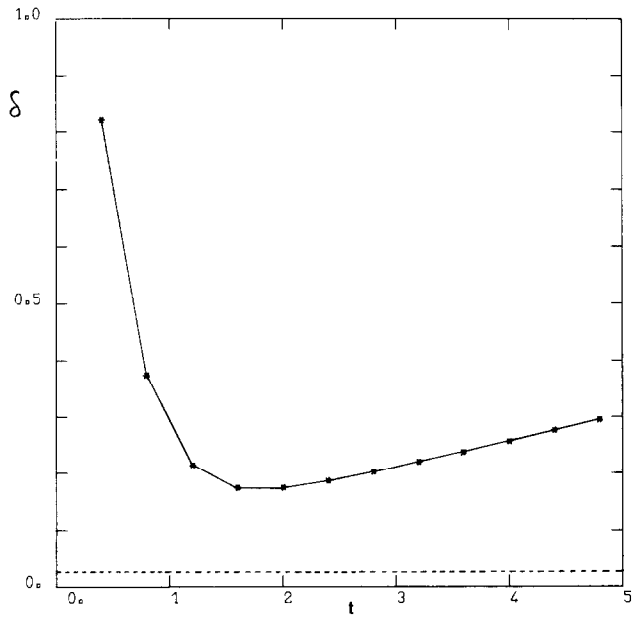

FIG. 3. Logarithmic decrement versus time for the viscous Burgers equation ($\nu = 0.05$). The dashed line shows the mesh size ($2\pi/256$).

as a function of time is plotted in Fig. 3. After decreasing to a minimum, it increases linearly in time in agreement with (3.15b).

IV. The Nonlinear Schrödinger Equation with Quartic Potential

The quartic nonlinear Schrödinger (NLS) equation reads

$$i\frac{\partial \psi}{\partial t}+\frac{\partial^2 \psi}{\partial x^2}+|\psi|^4\,\psi=0. \tag{4.1}$$

This equation preserves the L^2-norm and the so called "energy"

$$\mathscr{H}=\int\left(\left|\frac{\partial \psi}{\partial x}\right|^2-\frac{1}{6}|\psi|^6\right)dx. \tag{4.2}$$

The problem in $\mathbb{R}$ has been considered in [16, 33]. The solution cannot remain smooth for all time if the energy $\mathscr{H}$ is negative and the initial value of the variance

$$\mathscr{V}(0)=\int x^2\,|\psi_0(x)|^2\,dx \tag{4.3}$$

finite. This is a consequence of the estimate

$$\frac{d^2\mathscr{V}}{dt^2}(t)\leqslant 8\mathscr{H}. \tag{4.4}$$

Scaling laws for the singularity, which corresponds to a blow-up of the sup-norm of the solution, were proposed in [33]. For periodic boundary conditions there is no proof of existence of a singularity because estimate (4.4) does not hold and we have been led to investigate the singularity problem numerically.

We have integrated (4.1) with initial condition

$$\psi_0(x)=3.72\,\sin(2\pi x), \tag{4.5}$$

which gives $\mathscr{H}\approx -2.9$. We have used the temporal scheme [9]

$$i\frac{\psi^{n+1}-\psi^n}{\delta t}+\frac{1}{2}\left(\frac{d^2\psi^n}{dx^2}+\frac{d^2\psi^{n+1}}{dx^2}\right)+\frac{1}{4}(|\psi^n|^4+|\psi^{n+1}|^4)(\psi^n+\psi^{n+1})=0, \tag{4.6}$$

which exactly preserves both the L^2-norm and the energy $\mathscr{H}$. The scheme being implicit, (4.6) is solved by an iterative procedure of the kind described in [26]. We used a variable time step (10^{-4} for $0<t<0.35\times 10^{-2}$; 0.5×10^{-4} for

$0.35 \times 10^{-2} < t < 0.625 \times 10^{-2}$; 0.25×10^{-4} for $0.625 \times 10^{-2} < t < 0.6625 \times 10^{-2}$; 0.125×10^{-4} for $0.6625 \times 10^{-2} < t < 0.67125 \times 10^{-2}$).

The amplitude and the phase of the solution in the physical space are represented in Figs. 4a and 4b. The amplitude has a peaked shape which becomes more and more accentuated in time. The growth of the amplitude at maximum together with the narrowing of the peak suggest a local representation of the complex solution of the form ($\tilde{x}$ is the distance from the maximum):

$$\psi(\tilde{x}, t) = (1/f(t))\ \Psi((\tilde{x}/g(t)))\exp[i\phi(\tilde{x}, t)]. \tag{4.7}$$

In addition, we make the ansatz

$$g(t) = f^2(t), \tag{4.8}$$

the same as in the full-space problem [33]. If one had $f^2(t) = o[g(t)]$, the L^2-norm of the peak, which is order of $\sqrt{g}/f$, would grow indefinitely in time. In the opposite

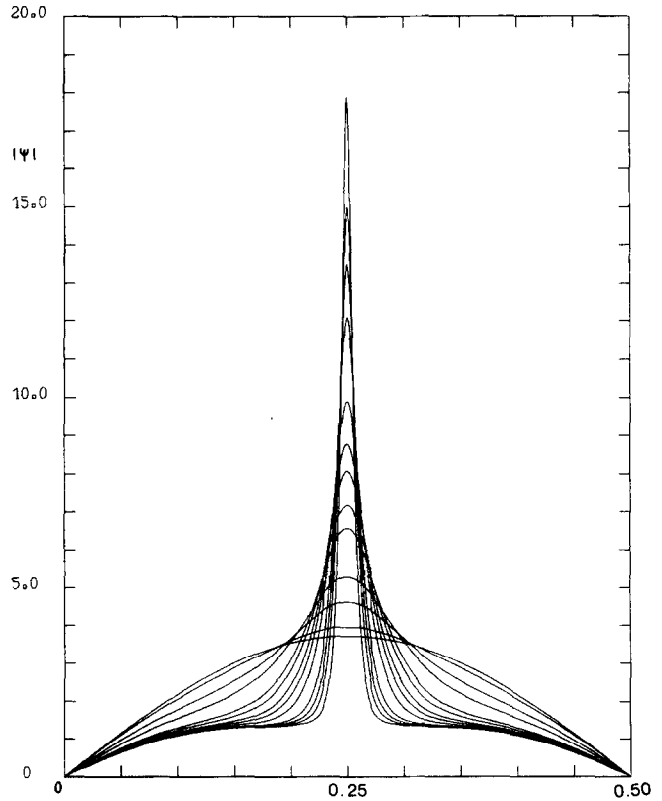

FIG. 4a. Amplitude of the solution of the nonlinear Schrödinger equation (NLS) with a quartic potential at times $t \times 10^3 = 0, 2, 2.75, 4.75, 5.75, 6, 6.25, 6.375, 6.5, 6.625, 6.6875, 6.7125$ (because of the symmetry of the solution, only half a period has been plotted).

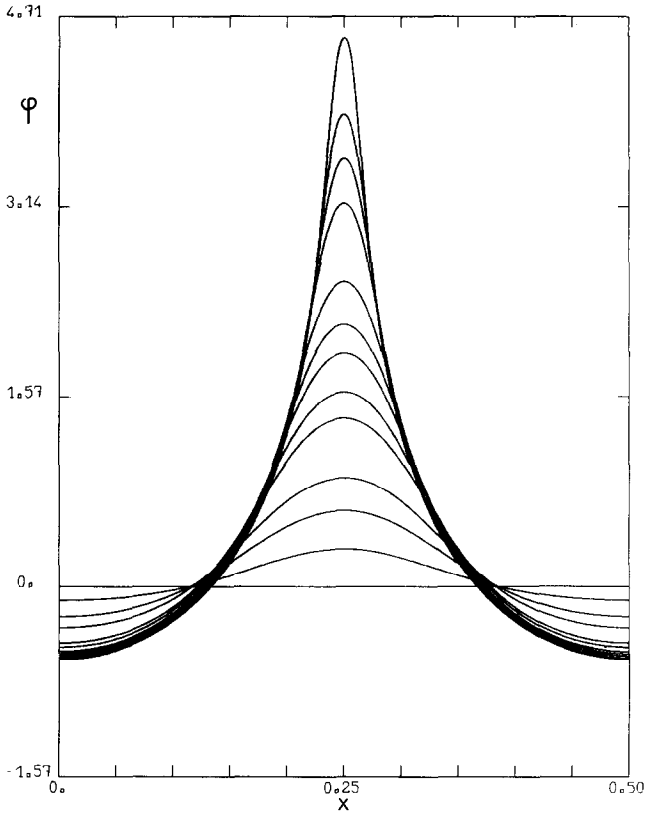

FIG. 4b. Phase of the solution of the NLS equation at the same times as in Fig. 4a.

situation, $g(t) = o[f^2(t)]$, the nonlinear term $|\psi^4|\psi$ would be negligible compared to the Laplacian of the amplitude. We shall see that the numerical data are compatible with ansatz (4.8).

The behavior of the phase ϕ around $\tilde{x} = 0$ can be represented by a parabola. Using (4.7) and (4.8), the real part of the Schrödinger equation may be written as

$$\frac{\partial}{\partial \tilde{x}} \left\{ \left[\frac{\partial \phi}{\partial \tilde{x}} - \frac{1}{2} \frac{\dot{g}(t)}{g(t)} \tilde{x} \right] \Psi^2 \left(\frac{\tilde{x}}{g(t)} \right) \right\} = 0. \tag{4.9}$$

Equation (4.9) shows that the term in the braces is independent of $\tilde{x}$. It is zero at $\tilde{x} = 0$ because Ψ is finite and $\partial\phi/\partial\tilde{x} = 0$ (ψ is an even function of $\tilde{x}$); hence it is zero for all $\tilde{x}$, and around $\tilde{x} = 0$ the phase may be represented by

$$\phi(\tilde{x}, t) \simeq \phi(0, t) + \frac{1}{4} \frac{\dot{g}(t)}{g(t)} \tilde{x}^2. \tag{4.10}$$

Hence, the behavior of the Fourier transform of $\psi(x, t)$ at large wavenumbers is determined by the analyticity properties of the amplitude profile Ψ. In particular, the logarithmic decrement $\delta(t)$ will be proportional to $g(t)$.

The odd Fourier modes are plotted in Fig. 5 (linear–log scales). The even modes are zero because of a symmetry of the problem. The behavior is clearly exponential at large wavenumbers. The odd modes have been fitted by

$$|\hat{\psi}_k(t)| \sim C(t)\, k^{-\alpha(t)} e^{-\delta(t)k}. \tag{4.11}$$

The maximum ψ_M of the amplitude is plotted versus $[\delta(t)]^{-1/2}$ at different times in Fig. 6. The linear variation, which occurs after a transient period of time, is in agreement with (4.8). Table III shows that the product $\psi_M^2 \delta$ is constant within 2%.

A value close to 0.5 is obtained for α (see table III); this corresponds to a complex singularity

$$\psi(z, t) \sim (z - z_*)^{-1/2}. \tag{4.12}$$

The nature of the singularity can also be derived from (4.1) by noticing that near a point where the solution is of the form $(z - z_*)^{\mu}$, the time derivative is negligible

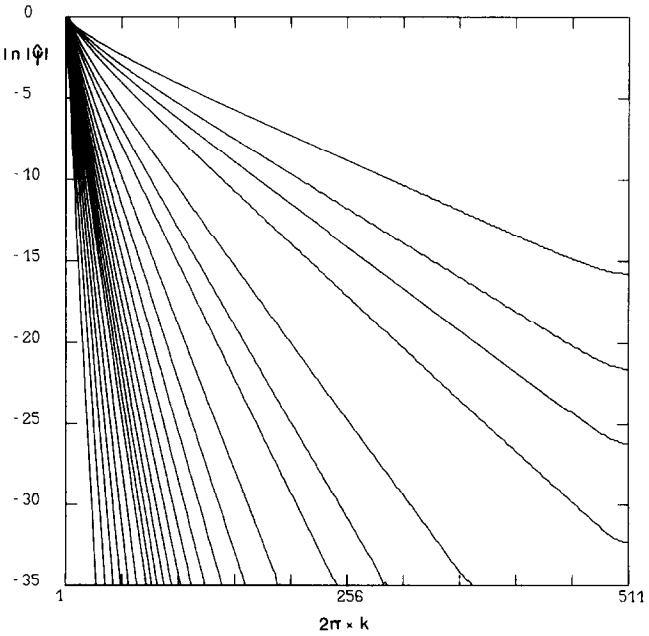

FIG. 5. Amplitude of the Fourier transform of the NLS equation from $t \times 10^3 = 0.5$ to 3.5 in steps of 0.5, from 3.75 to 6.25 in steps of 0.25, from 6.375 to 6.625 in steps of 0.125, and from 6.6875 to 6.7125 in steps of 0.03175.

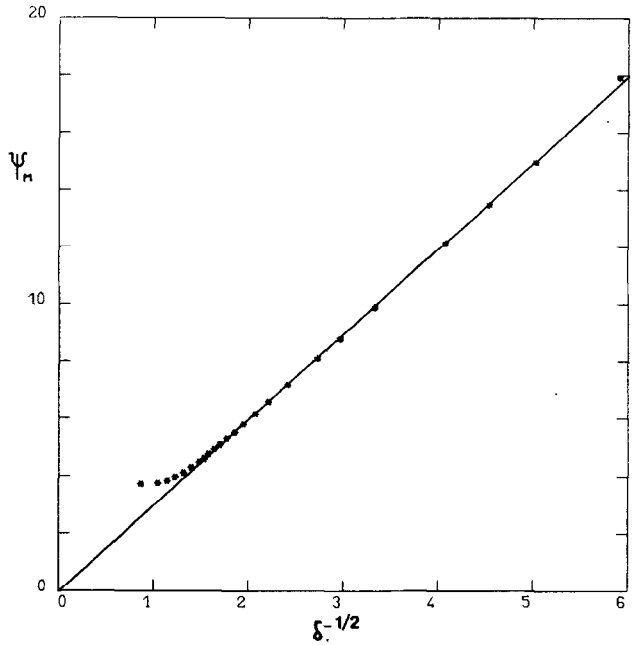

FIG. 6. Amplitude ψ_M at the maximum plotted versus the logarithmic decrement δ to the power $-\frac{1}{2}$ for the NLS equation at the same times as in Fig. 5.

TABLE III

Nonlinear Schrödinger Equation

$t \cdot 10^2$	$\psi_M^2 \delta$	α
0.375	9.12	0.48
0.425	9.	0.52
0.475	8.88	0.52
0.525	8.88	0.50
0.575	8.83	0.50
0.625	8.84	0.49
0.6375	8.73	0.51
0.65	8.79	0.49
0.66625	8.88	0.47
0.66875	8.95	0.47

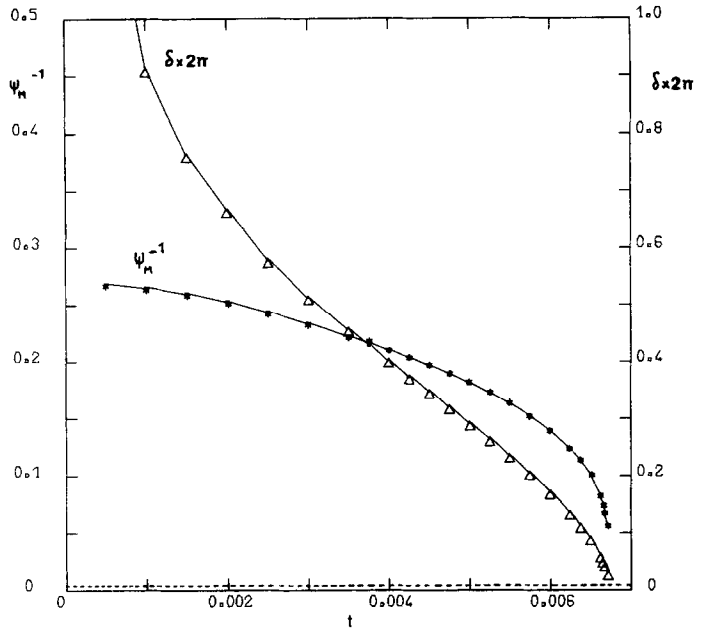

FIG. 7. Logarithmic decrement δ and inverse of the maximum amplitude ψ_M versus time for the NLS equation. The dashed line shows the mesh size.

when compared to the Laplacian. A value $\mu = -0.5$ is obtained by balancing the nonlinear and dispersive terms.

The temporal evolutions of the decrement δ and of the inverse of the maximum amplitude ψ_M are plotted in Fig. 7. Note the inflection point on the δ curve. A high resolution ($k_{max} = 512$) is necessary to reach a reasonably asymptotic regime. Figure 7 strongly suggests that after a finite time δ vanishes and ψ_M blows up.

The blow-up of ψ can be described quantitatively by extracting the time dependence of the scaling factors $f(t)$ and $g(t)$ from the numerical data. We have assumed time dependences of the form

$$1/\psi_M(t) \propto f(t) = C(t_* - t)^{\lambda}, \qquad \delta(t) \propto g(t) = C'(t'_* - t)^{\lambda'}. \tag{4.13}$$

The exponents λ and λ' were obtained in the following way: For different choices of λ and λ', $\psi_M^{-1/\lambda}$ and $\delta^{1/\lambda'}$ were fitted by linear laws using a least-squares method. Only the last 8 points, corresponding to the time interval $6.25 \times 10^{-3} \leqslant t \leqslant 6.7125 \times 10^{-3}$, were kept. Figure 8 shows the dispersions around these lines versus $1/\lambda$ and $2/\lambda'$. The positions of the minima differ by about 1% from the value $\lambda = \lambda'/2 = 4/7 \approx 0.57$ obtained by Zakharov and Synakh from an asymptotic analysis of the full space problem. When $\lambda = \lambda'/2$ is in the range (0.56–0.58), the singularity times t_* and t'_* differ by at most 0.1%. Figure 9 displays straight-line fits of $\delta^{1/\lambda'}$ and $\psi_M^{-1/\lambda}$ with $\lambda =$

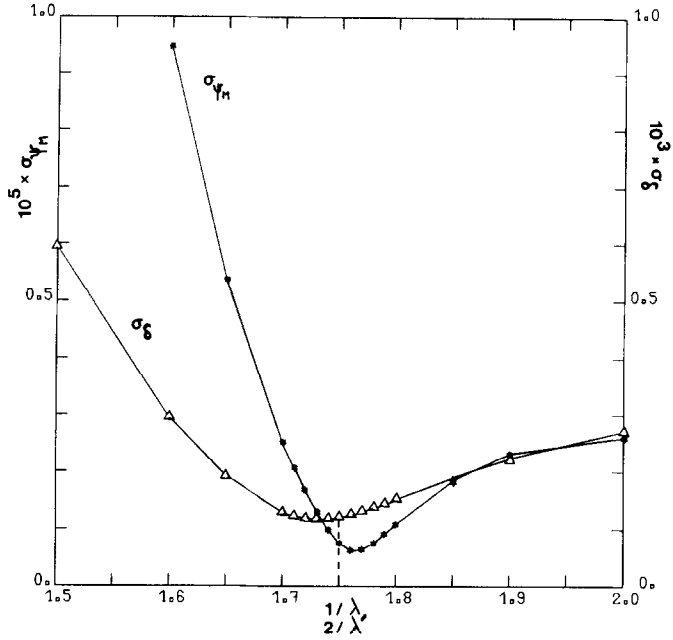

FIG. 8. Dispersion σ_{ψ_M} and σ_δ of $|\Psi_M^{-1/\lambda} - C(t_* - t)|$ and $|\delta^{1/\lambda'} - C'(t'_* - t)|$ versus $1/\lambda$ and $2/\lambda'$ in the time interval $6.25 \times 10^{-3} \leqslant t \leqslant 6.7125 \times 10^{-3}$. The dashed line shows the value $\lambda = 4/7$.

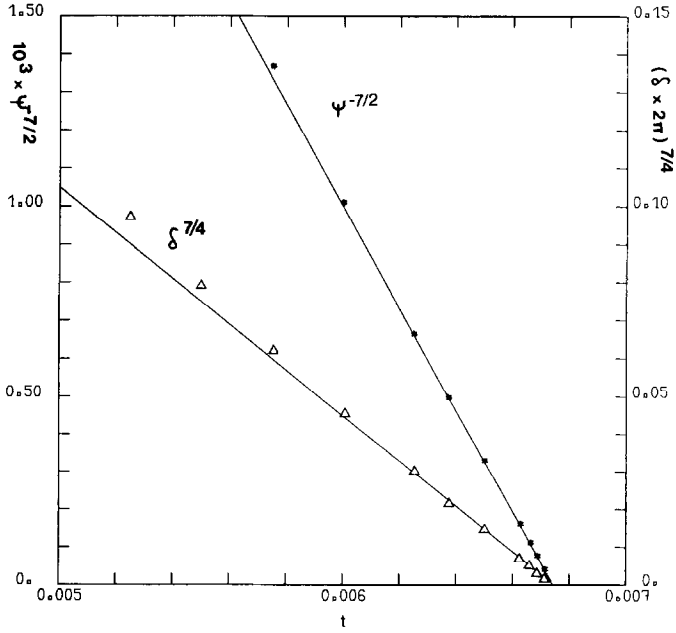

FIG. 9. Nonlinear Schrödinger equation: $\Psi_M^{-7/2}$ and $\delta^{7/4}$ versus time, (△) and (∗): numerical data; (—) least-squares fit for $\lambda = \frac{2}{7}$ and $\lambda' = \frac{4}{7}$.

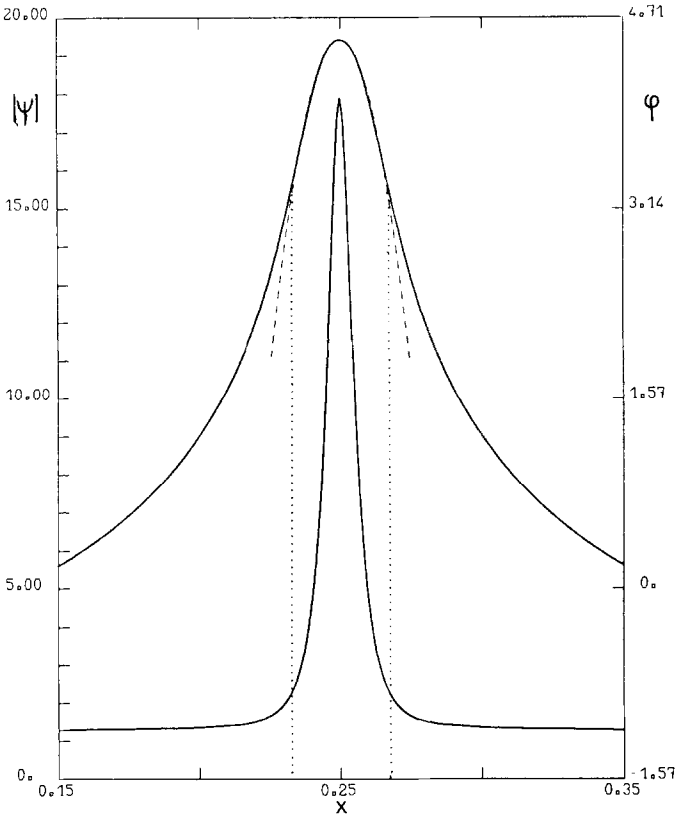

FIG. 10. Amplitude and phase of the NLS equation at time $t = 6.7125 \times 10^{-3}$. The dashed line is a parabolic fit of the phase according to (4.10) with $\dot{g}(t)/g(t) = \frac{4}{7}(t_* - t)^{-1}$. The vertical dotted lines indicate the range of validity.

$\lambda'/2 = 4/7$. Figure 10 shows the phase fitted by the parabola (4.10) with $\dot{g}(t)/g(t) = 4/7\ (t_* - t)^{-1}$ at time 6.7125×10^{-3}. Note that the totality of the amplitude peak falls inside the range of validity of (4.10).

Our numerical results are compatible with ansatz (4.8) and suggest that the nonlinear Schrodinger equation with quartic potential and periodic boundary conditions blows up in a finite time when the energy is negative with the same scaling laws as those of the full-space problem.

V. Two-Dimensional Euler Equation

In this section, we apply a multi-dimensional extension of the method presented in Section II to the two-dimensional Euler equation with periodic boundary conditions:

$$\frac{\partial u}{\partial t} + u \cdot \nabla u = -\nabla p, \qquad \nabla \cdot u = 0,$$

$$u(\mathbf{x}, 0) = u_0(\mathbf{x}), \qquad \mathbf{x} \in [0, 2\pi]^2. \tag{5.1}$$

Existence for all times of a classical solution has been known for a long time [19, 20, 31]. It results from the conservation of vorticity, $\omega = \operatorname{curl} u$, along the fluid trajectories. A sketch of the proof is given in [12, 28]. Analyticity for all times was proved in [2]. It is shown in this reference that if the (periodic) initial condition $u_0(\mathbf{x})$ can be continued as an analytic function in a strip $|\operatorname{Im} \mathbf{x}| < d_0$, then, for any real time, the solution remains analytic in some strip $|\operatorname{Im} \mathbf{x}| < D(t)$ which does not go to zero faster than an exponential of an exponential. Here $D(t)$ is actually a lower bound for the analyticity strip $d(t)$. As we shall now see, the numerical evidence is that the decrease of $d(t)$ is actually exponential.

For the numerical experiment, we have chosen the initial condition (proposed in [25])

$$u_1 = -\sin y - \sin 2y, \qquad u_2 = \sin x + \sin 2x. \tag{5.2}$$

Figure 11 shows the contours of the initial vorticity. Deterministic initial conditions

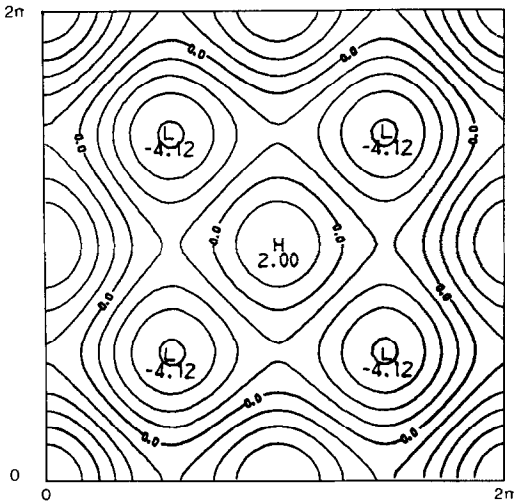

FIG. 11. Two-dimensional Euler equation. Vorticity contours of initial condition (5.2); H and L denote maximum and minimum, respectively.

rather than random ones (as in [3, 8, 10, 18, 22]), were chosen because we are here basically interested in the dynamics and analytical structure of individual realizations.

The calculation was performed with $(256)^2$ Fourier modes (maximum wavenumber $k_{\max} = 128$ after circular truncation). No dealiasing was made. For the temporal scheme we chose a stabilized leapfrog with a time step $\Delta t = 2 \times 10^{-3}$.

Figure 12 shows the angle-averaged energy spectrum

$$E(K) = \sum_{K<k<K+1} |\hat{v}_k|^2 \tag{5.3}$$

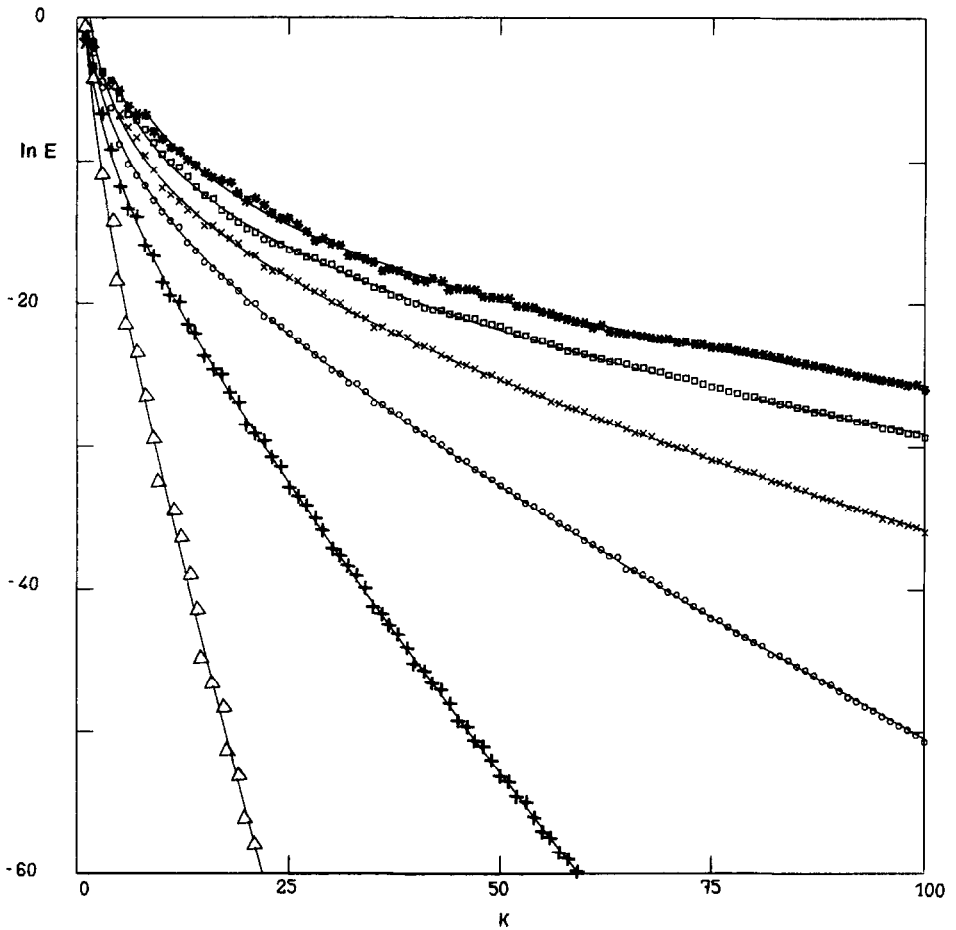

FIG. 12. Angle-averaged energy spectrum of the two-dimensional Euler equation in linear-log scales at equally spaced times between $t = 0.2$ and 2.2 in steps of 0.4 for initial condition (5.2).

in linear–log scales up to $t = 2.2$. The solid lines are least-square fits to the logarithm of the energy spectrum, assuming the functional form

$$E(K) = C(t)\, K^{-\alpha(t)} e^{-\delta(t)K}. \tag{5.4}$$

An exponential decay of the energy spectrum is visible at large wavenumbers; the small oscillations come from truncation and aliasing errors and also from interferences of singularities.

The time evolution of the logarithmic decrement is shown in Fig. 13 for $t \leqslant 2.2$. Clearly, $\delta(t)$ decays exponentially. The characteristic time of decay (here near 0.5) provides a typical dynamical time scale for the inviscid problem. This exponential is almost insensitive to the precise choice of the fitting range of wavenumbers. Figure 13 corresponds to a fit in the range $8 \leqslant k \leqslant 100$. At times $t > 2.2$, δ becomes much smaller than the mesh size and the smallest scales cannot be safely resolved. The logarithmic decrement $\delta(t)$ obtained in this way gives a numerical estimate of the width of the analyticity strip $d(t)$. Indeed, if the analyticity strip were larger than $\delta(t)$, the energy spectrum would decrease faster than $e^{-\delta(t)K}$, in contradiction with the observed behavior (5.4).

The vorticity contours at $t = 2$ are shown in Fig. 14. Note the formation of thin layers of high vorticity gradient which probably reflect the existence of nearby complex singularities. The formation of such layers, across which the vorticity is

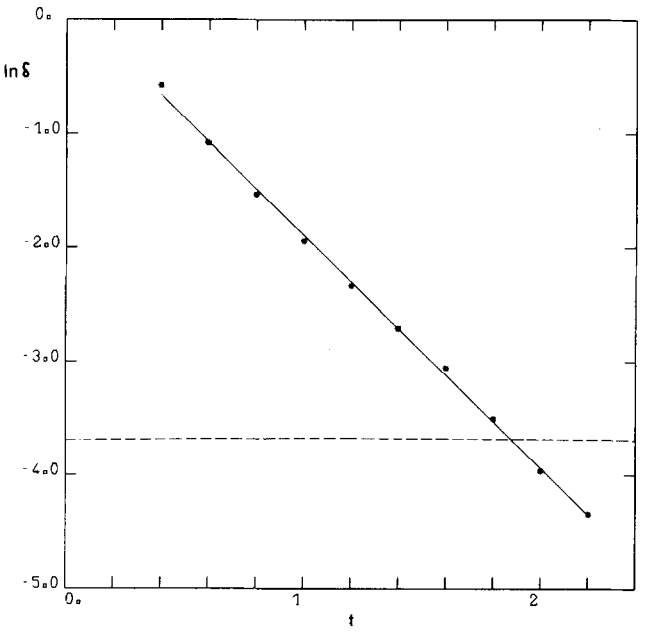

FIG. 13. Logarithmic decrement versus time of the two-dimensional Euler equation. The dashed line shows the mesh size ($2\pi/256$).

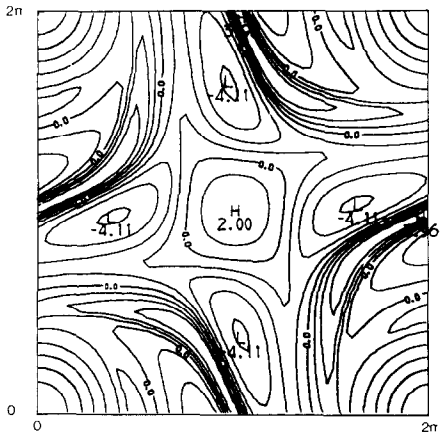

FIG. 14. Two-dimensional Euler equation. Vorticity contours at time $t = 2$.

nearly discontinuous, was predicted by Saffman [29] using a vorticity advection argument. Actual vorticity discontinuities should produce a k^{-4} energy spectrum. We have not observed any significant k^{-4} range; recent simulations at higher resolution (512^2) [5] have not substantially changed this situation.

As for an enstrophy cascade range, possibly following a k^{-3} law [4, 21] or a steeper law [3], it is very doubtful that it can be observed without performing some kind of statistical averaging which requires a driving process and very long integration times.

VI. FURTHER APPLICATIONS

The method presented here has been applied recently to other nonlinear evolution equations. In [13, 25] evidence is given suggesting regularity for all times of the inviscid MHD flow in two dimensions. In contrast with the Euler equation, the MHD equations do not conserve the vorticity; therefore the Wolibner [31] proof of global regularity is inapplicable. For the cubic Schrödinger equation in two dimensions, blow-up problems and the corresponding scaling laws are considered in [30]; in particular, evidence for blow up is obtained for periodic boundary conditions. The three-dimensional Euler equation with the Taylor–Green vortex as initial condition has been integrated numerically using 256^3 Fourier modes in [6]; an exponential decrease of the width of the analyticity strip is observed during the period of time when the computation is reliable. However, as pointed out in [6], this behavior may be transient. A higher resolution seems necessary in this case to safely decide whether or not the three-dimensional Euler equation develops a real singularity.

ACKNOWLEDGMENTS

We have greatly benefitted from stimulating discussions with C. Bardos, M. E. Brachet, J. D. Fournier, U. Frisch, F. Pham, and A. Pouquet. The two-dimensional Euler equation was integrated on the CRAY 1 computer at the National Center for Atmospheric Research, which is sponsored by the National Science Foundation.

REFERENCES

1. V. ARNOLD, "Chapitres supplémentaires de la théorie des équations differentielles ordinaires," French translation, Mir, Moscow, 1980.
2. C. BARDOS, S. BENACHOUR, AND M. ZERNER, *C. R. Acad. Sci. Paris Sér. A–B* **282** (1976), A 995.
3. C. BASDEVANT, B. LEGRAS, R. SADOURNY, AND M. BÉLAND, *J. Atmos. Sci.* **38** (1981), 2305.
4. G. K. BATCHELOR, *Phys. Fluids* (Suppl. 2) **12** (1969), 233.
5. M. E. BRACHET, unpublished, 1982.
6. M. E. BRACHET, D. I. MEIRON, S. A. ORSZAG, B. NICKEL, R. MORF, AND U. FRISCH, Small-scale structure of the Taylor–Green vortex, *J. Fluid Mech.* (1983), in press.
7. G. F. CARRIER, M. KROOK, AND C. E. PEARSON, "Functions of a Complex Variable," McGraw–Hill, New York, 1966.
8. G. S. DEEM AND N. J. ZABUSKY, *Phys. Rev. Lett.* **27** (1971), 396.
9. L. M. DEGTYAREV, *Sov. Phys. Dokl.* **24** (1979), 716.
10. B. FORNBERG, *J. Comput. Phys.* **25** (1977), 1.
11. J. D. FOURNIER AND U. FRISCH, "L'équation de Burgers déterministe et statistique," 1982; *J. Méc. Théor. Appl.* (1983), in press.
12. U. FRISCH, Fully developed turbulence and singularities, *in* "Les Houches Summer School," 1981, North-Holland to appear.
13. U. FRISCH, P. L. SULEM, A. POUQUET, AND M. MENEGUZZI, "The Dynamics of Two-Dimensional Ideal Magnetohydrodynamics," *J. Méc. Théor. Appl.*, special issue (1983) on two-dimensional turbulence, in press.
14. U. FRISCH AND R. MORF, *Phys. Rev. A* **23** (1981), 2673.
15. D. S. GAUNT AND A. J. GUTTMANN, *in* "Phase Transition and Critical Phenomena" (C. Domb and M. S. Green, Eds.), Vol. 3, p. 81, Academic Press, London, 1974; G. S. RUSHBROOKE, G. A. BAKER, JR., AND P. S. WOOD, p. 246.
16. R. T. GLASSEY, *J. Math. Phys.* **18** (1977), 1794.
17. D. GOTTLIEB AND S. A. ORSZAG, "Numerical Analysis of Spectral Methods," SIAM, Philadelphia, Pa., 1977.
18. J. R. HERRING, S. A. ORSZAG, R. H. KRAICHNAN, AND D. G. FOX, *J. Fluid Mech.* **66** (1974), 417.
19. E. HÖLDER, *Math. Z.* **37**(1933), 327.
20. T. KATO, *Arch. Rat. Mech. Anal.* **25** (1967), 188.
21. R. H. KRAICHNAN, *Phys. Fluids* **10** (1967), 1417; *J. Fluid. Mech.* **47** (1971), 525.
22. D. K. LILLY, *J. Fluid. Mech.* **45** (1971), 395.
23. D. I. MEIRON, G. R. BAKER, AND S. A. ORSZAG, *J. Fluid Mech.* **114** (1982), 283.
24. R. H. MORF, S. A. ORSZAG, AND U. FRISCH, *Phys. Rev. Lett.* **44** (1980), 572.
25. R. H. MORF, S. A. ORSZAG, D. I. MEIRON, U. FRISCH, AND M. MENEGUZZI, *in* "Proc. Seventh. Intern. Conf. Numeric. Meth. in Fluid Dynamics," Lecture Notes in Physics No. 141, p. 282, Springer-Verlag, Berlin, 1981.
26. S. A. ORSZAG, *J. Comput. Phys.* **37** (1980), 70.
27. S. A. ORSZAG AND C. M. TANG, *J. Fluid Mech.* **90** (1979), 129.
28. H. A. ROSE AND P. L. SULEM, *J. Phys. Paris* **39** (1978), 441.

29. P. G. SAFFMAN, *Stud. Appl. Math.* **50** (1971), 377.
30. P. L. SULEM, C. SULEM, AND A. PATERA, "Numerical Simulation of Singular Solutions to the Two-Dimensional Cubic Schrödinger Equation," 1982, preprint.
31. W. WOLIBNER, *Math. Z.* **37** (1933), 727.
32. N. ZABUSKY, *J. Comput. Phys.* **43** (1981), 195.
33. V. E. ZAKHAROV AND V. S. SYNAKH, *Sov. Phys.–JETP* **41** (1976), 465.